JOURNAL OF GEOPHYSICAL RESEARCH, VOL. 111, D14S90, doi:10.1029/2005JD006341, 2006

Shortwave radiative closure studies for clear skies during the Atmospheric Radiation Measurement 2003 Aerosol Intensive Observation Period

J. J. Michalsky,[1] G. P. Anderson,[2] J. Barnard,[3] J. Delamere,[4] C. Gueymard,[5] S. Kato,[6] P. Kiedron,[7] A. McComiskey,[8] and P. Ricchiazzi[9]

Received 7 June 2005; revised 2 March 2006; accepted 4 April 2006; published 20 July 2006.

[1] The Department of Energy's Atmospheric Radiation Measurement (ARM) program sponsored a large aerosol intensive observation period (AIOP) to study aerosol during the month of May 2003 around the Southern Great Plains (SGP) Climate Research Facility (CRF) in north central Oklahoma. Redundant measurements of aerosol optical properties were made using different techniques at the surface as well as in vertical profile with sensors aboard two aircraft. One of the principal motivations for this experiment was to resolve the disagreement between models and measurements of diffuse horizontal broadband shortwave irradiance at the surface, especially for modest aerosol loading. This paper focuses on using the redundant aerosol and radiation measurements during this AIOP to compare direct beam and diffuse horizontal broadband shortwave irradiance measurements and models at the surface for a wide range of aerosol cases that occurred during 30 clear-sky periods on 13 days of May 2003. Models and measurements are compared over a large range of solar-zenith angles. Six different models are used to assess the relative agreement among them and the measurements. Better agreement than previously achieved appears to be the result of better specification of input parameters and better measurements of irradiances than in prior studies. Biases between modeled and measured direct irradiances are in the worst case 1%, and biases between modeled and measured diffuse irradiances are less than 1.9%.

Citation: Michalsky, J. J., G. P. Anderson, J. Barnard, J. Delamere, C. Gueymard, S. Kato, P. Kiedron, A. McComiskey, and P. Ricchiazzi (2006), Shortwave radiative closure studies for clear skies during the Atmospheric Radiation Measurement 2003 Aerosol Intensive Observation Period, *J. Geophys. Res.*, *111*, D14S90, doi:10.1029/2005JD006341.

1. Introduction

[2] Achieving agreement between clear-sky shortwave broadband irradiance models and measurements is one requirement for validating models, and it is the first step to further use of these models in more complicated cloudy-sky analyses. However, recent efforts to achieve broadband shortwave radiative closure have met with some difficulties. *Kato et al.* [1997] looked at clear-sky data in the mid 1990s and found that direct beam irradiance (hereafter, direct irradiance) models and measurements agreed well. *Halthore et al.* [1997] reached a similar conclusion. *Kato et al.*'s [1997] diffuse horizontal broadband shortwave irradiance (hereafter, diffuse irradiance) measurements, however, were well below the modeled irradiance even though the uncertainties in the inputs and errors due to model assumptions were taken into account. *Halthore et al.* [1998] concluded, likewise, that models of diffuse irradiance were higher than measurements. This led to a reassessment of offsets in thermal pyranometers caused by the temperature gradient between the dome and thermopile in pyranometers that had been noted decades earlier [e.g., *Gulbrandsen*, 1978], but largely ignored. A series of papers resolved the offset issue by proposing methods to correct the error [*Bush et al.*, 2000; *Haeffelin et al.*, 2001; *Dutton et al.*, 2001; *Michalsky et al.*, 2003a]. *Halthore and Schwartz* [2000] found that even with corrected offsets, diffuse irradiance measurements were persistently lower than models. *Barnard and Powell* [2002] confirmed the *Halthore and Schwartz* [2000] result for the Southern Great Plains (SGP) Climate Research Facility (CRF), however, using data from the North Slope of Alaska, Atmospheric Radiation Measurement (ARM) site

[1]Earth System Research Laboratory, NOAA, Boulder, Colorado, USA.
[2]Air Force Research Laboratory/Battlespace Surveillance Innovation Center, U.S. Air Force, Boulder, Colorado, USA.
[3]Pacific Northwest National Laboratory, Richland, Washington, USA.
[4]Atmospheric and Environmental Research, Inc., Lexington, Massachusetts, USA.
[5]Solar Consulting Services, Inc., Colebrook, New Hampshire, USA.
[6]Center for Atmospheric Sciences, Hampton University, Hampton, Virginia, USA.
[7]Atmospheric Sciences Research Center, State University of New York, Albany, New York, USA.
[8]Cooperative Institute for Research in Environmental Sciences, University of Colorado, Boulder, Colorado, USA.
[9]Institute for Computational Earth System Science, University of California, Santa Barbara, California, USA.

0148-0227/06/2005JD006341$09.00

near Barrow, they were able to achieve closure to within the measurement and model uncertainty. In a recent paper using improved aerosol property inputs to the model, *Halthore et al.* [2004] were still unable to achieve closure at the SGP CRF in northern Oklahoma. In another recent paper where model input aerosol optical properties were carefully scrutinized, *Henzing et al.* [2004] were able to achieve closure between direct beam measurements and models, but found that models produced much higher diffuse irradiance for a midlatitude site in the Netherlands.

[3] This paper uses data from a major aerosol field experiment conducted between 5 May 2003 and 30 May 2003 at and above the ARM SGP CRF, which is located midway between Lamont and Billings, Oklahoma, at 36.61°N and 97.49°W. A major goal of this aerosol intensive observation period (AIOP) was to obtain redundant measurements of each aerosol optical property needed as model input to radiative transfer codes. This paper features computations of direct and diffuse irradiance using six radiative transfer codes and carefully scrutinized inputs. Notable improvements include better asymmetry parameters and better spectral surface albedo specifications than in prior studies. The comparisons cover a wide range of aerosol optical thicknesses, solar zenith angles, and water vapor amounts. These model results are compared with careful measurements of direct and thermal-offset-corrected diffuse irradiances.

[4] In section 2 the data used as input to the models and the radiation data used to compare to model calculations are described. The six models that are used to generate the results for the 30 cases are described in section 3. Results of the model-model and model-measurement comparisons are shown in section 4. Major conclusions are discussed in the final section.

2. Model Data Input and Radiation Measurements

[5] Skies were screened for totally cloud-free periods using three sources of data. First, time series plots of broadband direct and diffuse data were used to screen for clear skies. This was followed with plots of the multifilter rotating shadow-band radiometer (MFRSR) 870-nm diffuse data [*Harrison et al.*, 1994]. This wavelength has little Rayleigh scattering, and even light cirrus noticeably affects the shape of the time series plots. A final step was to use sky images from the YES, Inc. Total Sky Imager (TSI) to confirm the selection of clear-sky period identifications. Thirty cases were identified that included low to high sun angles and aerosol optical thickness that ranged over those typically observed for this site. Extremely low values of aerosol optical thickness (<0.05) were not and are not generally observed in May.

[6] The most important input variables in clear-sky solar radiation modeling of surface irradiance include aerosol information, specifically, column aerosol optical depth, single scattering albedo, and asymmetry parameter, all as a function of wavelength. The other key variables for clear-sky modeling are, in approximate order of importance, column water vapor, the spectral albedo of the surface that surrounds the sites where irradiance measurements are made, and column ozone.

[7] Aerosol optical depth measurements were made with a normal incidence multifilter radiometer (NIMFR), which is a modified MFRSR that looks directly at the sun with a 5.7° field of view. Optical depths are measured at five wavelengths including 415, 500, 615, 673, and 870 nm. Measurements are made every 20 s during all daylight hours. CIMEL Sun photometer measurements are also made at the ARM CRF as part of the AERONET network [*Holben et al.*, 1998]. For 13 of the 30 cases we compared CIMEL and NIMFR measurements at or near three wavelengths: 500, 670, and 870 nm. Of the 39 comparisons two were not within the 95% uncertainty limits, about as expected, and there was negligible bias between the measurement sets. This is based on a CIMEL 95% aerosol optical depth uncertainty of 0.02 [*Schmid et al.*, 1999] and a slightly larger assumed NIMFR 95% uncertainty of 0.02–0.025 given that the NIMFR has a larger field of view than the CIMEL. Further, *Schmid et al.* [2006] compared NIMFR measurements with the 14-channel Ames Airborne Tracking Sunphotometer (AATS-14) on 12 occasions when the instrument flew about 90 m above the ground-based NIMFR. They report root-mean-squared differences and biases that were slightly better than those between the AATS-14 and two CIMEL Sun photometers that operated during the campaign. The NIMFR aerosol optical depth was used in all calculations.

[8] Values for single scattering albedo (ϖ_o) and asymmetry parameter (g) used in the radiative transfer calculations were derived from ground-based in situ measurements made with the CRF's Aerosol Observing System (AOS). The AOS consists of several inline instruments that measure aerosol properties for particle diameters less than 10 μm and for particle diameters less than 1 μm. Sample air is pulled through a 10 m stack above the measurement site to avoid ground contamination. The sample is heated so that the air remains at a low relative humidity (<40%) within the system to avoid the effects of hygroscopic growth on aerosol optical properties. Aerosol absorption is measured at 565 nm using a Particle Soot/Absorption Photometer (PSAP) and reported as an absorption coefficient (σ_{ap}) in m^{-1}. Aerosol scattering is measured at three wavelengths, 450, 550, and 700 nm, using two TSI, Inc. Model 3563 Integrating Nephelometers operated in series. The first nephelometer is held at a low relative humidity (<40%) while the second is ramped between 40 and 90% relative humidity every hour. Data from the first nephelometer are used to report dry scattering (σ_{sp}) and backscattering (σ_{bsp}) coefficients in m^{-1}. A humidification factor is computed with data from the second nephelometer, which is then used with the ambient relative humidity at the time of the measurement to adjust the optical properties for hygroscopic growth. A comprehensive explanation of the AOS is given by *Sheridan et al.* [2001]. On occasion, when AOS data were unavailable, data from a backup system in the guest instrument facility (GIF) within 200 m of the CRF were used. The two systems produced data that agreed to within their uncertainties when both were operating.

[9] All scattering and backscattering data for particle diameters less than 10 μm were adjusted to ambient humidity conditions for the model calculations. The single scattering albedo (ϖ_o), the ratio of scattering to extinction, was computed from the above measurements ($\varpi_o = \sigma_{sp}/(\sigma_{sp} + \sigma_{ap})$).

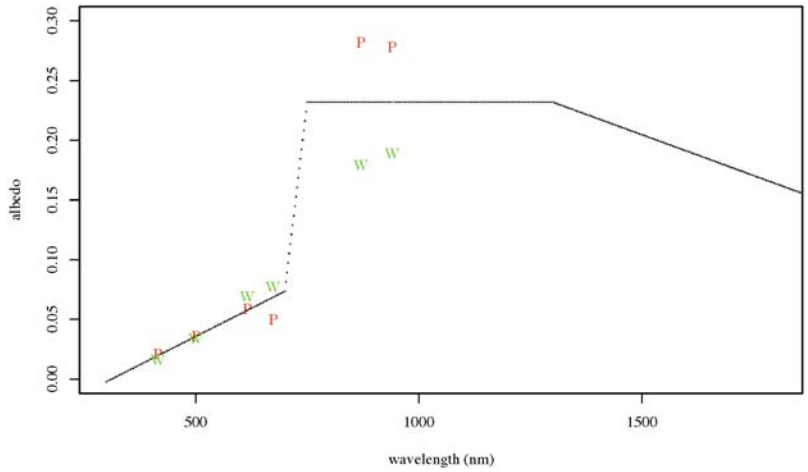

Figure 1. Parameterized surface albedo input (dotted black line). The individual measurements of wheat (W) and pasture (P) surface albedos are also shown.

The uncertainty associated with ϖ_o ranges from 0.036 to 0.049 for high- and low-scattering cases [*Sheridan et al.*, 2002]. The asymmetry parameter, the cosine weighted integral of the aerosol phase function, is derived from an empirical relationship using the backscattered fraction ($b = \sigma_{bsp}/\sigma_{sp}$) [*Wiscombe and Grams*, 1976] that assumes the Henyey-Greenstein phase function. Uncertainties for b range from 0.012 to 0.018 for high- and low-scattering cases [*Sheridan et al.*, 2002]. Comparisons of the derivations of g from different data sources and their corresponding uncertainties are presented in a paper based on data from this IOP [*Andrews et al.*, 2006].

[10] The water vapor column was obtained from the ARM data archive http://www.archive.arm.gov. These measurements are made every 20 s using a microwave radiometer, however, the 5-min-averaged data are used for this study. The derivation of and uncertainty in column water vapor (±0.05 cm) is explained by *Liljegren* [1994]. The column water vapor was adjusted downward from the current ARM archived values by 3% following a suggestion by *Liljegren et al.* [2005] based on improved microwave retrievals. Ozone data are obtained from the Total Ozone Mapping Spectrometer (TOMS) web site http://toms.gsfc.nasa.gov. When TOMS data were not available (two cases), Dobson data from Boulder, Colorado, obtained from the Climate Monitoring and Diagnostics Laboratory (CMDL) website http://www.cmdl.noaa.gov/ozwv/dobson were used. Using the mean difference between the TOMS and CMDL data for the month of May 2003 results in a negligible change of 0.1% in diffuse and a 0.05% change in direct.

[11] Spectral surface albedo input data were parameterized from the two downward looking multifilter radiometer (MFR) heads that are on the 10-m tower over ungrazed pasture and at the 25-m level of the 60-m tower over a wheat field. MFR data were divided by uplooking MFRSR data to determine surface albedos at six wavelengths. Equal weighting of the surface albedos used in the calculations was based on the subjective observation that the site is surrounded mostly by wheat and pasture in equal proportions. The parameterization used for the surface albedo between 300 and 3000 nm is described by *Michalsky et al.* [2003b]. A straight line is fit between 300 and 700 nm using the four shortest wavelengths (415, 500, 615, and 673 nm) from the two MFRs. A constant value is determined using the average value of the two longest wavelengths (870 and 940 nm) from the two MFRs and used for all wavelengths between 750 and 1300 nm. A line connects the 700 and 750 nm points from each fit. Finally, a line connects the 1300 nm point and zero surface albedo at 3000 nm on the basis of general tendencies for vegetation. Figure 1 illustrates how the wavelength-dependent surface albedo was determined for a single case. Since clear-sky surface albedos show solar-zenith angle and wavelength dependencies, the surface albedo is determined for each observation.

[12] The ground-based direct beam and diffuse horizontal shortwave irradiance data used in model comparisons were obtained from the CRF's radiation calibration facility (RCF) and guest instrument facility (GIF) that are separated by no more than 200 m. An absolute cavity radiometer makes the preferred measurement of direct beam irradiance with an uncertainty of 0.4% or about 3–4 W/m^2. Cavity measurements were made from the RCF for seven of the 30 cases studied. For the other direct beam measurements a pyrheliometer, Eppley model NIP, labeled A on the GIF observing stand was used with an uncertainty of about 1–1.5% or 8–12 W/m^2. The diffuse horizontal irradiance data were obtained from two instruments on the GIF observing stand. The diffuse value used was an average of an Eppley 8-48 shaded pyranometer, which has no offset, and an offset-corrected Kipp & Zonen CM22. The small offset correction applied in the latter case is a two-parameter fit as explained by *Michalsky et al.* [2005]. The estimated uncertainty in diffuse irradiance is about 4% or about 4 W/m^2.

3. Models Used in the Downwelling Shortwave Calculations

[13] The models used for the comparisons have low to moderate spectral resolution. The modeled direct beam and diffuse horizontal spectral irradiances are spectrally integrated to compare with broadband shortwave measurements. The extraterrestrial spectral irradiance assembled by *Gueymard* [2004] was used as the input spectrum, except for one model, and this input irradiance was scaled to the

Table 1. Descriptions of Model Features

Model	λ Range, nm	λ Resolution	Surface Albedo	Radiative Transfer	Web Site	References
RAPRAD	240–4600	32 discrete bands	300–3000 nm, as specified, with fixed 300 nm and 3000 nm values above and below these λs	correlated k and Delta-2 stream		*Toon et al.* [1989] and *Kato et al.* [1999]
MODTRAN 4.9	280–4000	5 cm^{-1}	same as above	correlated k and DISORT, 8-stream	http://www.vs.afrl.af.mil/productlines/ir-clutter/modtran4.aspx	*Anderson et al.* [2000]
SMARTS 2.9.5	280–4000	0.5 nm if < 400 nm, 1 nm if 400–1705 nm, 5 nm if > 1705 nm	same as above	modified 2-stream	http://rredc.nrel.gov/solar/models/SMARTS/	*Gueymard* [1995, 2001]
RRTM_SW, version 2.5	263–3846	14 discrete bands	used albedos at 415, 500, 615, 673, 870, and 940 nm and scaled with tabulated vegetative albedos	correlated k and DISORT, 8-stream	http://rtweb.aer.com	*Mlawer and Clough* [1998] and *Clough et al.* [2004]
SBDART 2.4	250–4500	variable with higher resolution at shorter wavelengths	300–3000 nm, as specified, with zero values below 300 and above 3000 nm	DISORT, 4-stream	http://www.crseo.ucsb.edu/esrg/pauls_dir	*Ricchiazzi et al.* [1998]
SBMOD 1.0	280–2950	5 nm	300–3000 nm, as specified, with zero values below 300 and above 3000 nm	correlated k and DISORT, 8-stream	http://www.crseo.ucsb.edu/esrg/pauls_dir	*Yang et al.* [2000]

actual solar distance. A surface albedo file that spanned the 300–3000 nm wavelength region was provided for each case. Table 1 contains information regarding the models and how inputs were applied for the 30 cases in this study.

[14] Correlated k distribution tables used in the rapid radiative (RAPRAD) transfer model [*Toon et al.*, 1989] were built on the basis of the high-resolution transmission molecular absorption database HITRAN 2000 [*Rothman et al.*, 2003] using a line-by-line radiative transfer model (LBLRTM [*Clough et al.*, 2004]). Absorption by water vapor, ozone, carbon dioxide and oxygen is included [*Kato et al.*, 1999]. To avoid assuming multiplication properties [*Goody and Yung*, 1989] for overlapping bands, the minor gas concentration was fixed and tables built as a function of pressure, temperature and concentration of major gases. Because the multiplicative rule gives the minimum transmission, the direct irradiance is larger by 0.4% compared to the direct irradiance using the multiplicative assumption.

[15] RAPRAD was run with some modifications to the specified inputs. To extrapolate measured single scattering albedos and asymmetry parameters at 550 nm to other wavelengths, the single scattering albedo and asymmetry parameter are computed with Mie theory using the refractive index of sulfate [*d'Almeida et al.*, 1991], a mode radius of 0.1 μm, and assuming a lognormal distribution with a standard deviation of 1.4 μm. These values are then scaled by the ratio of the computed-to-measured values at 550 nm.

[16] The moderate resolution radiative transfer model MODTRAN™4.9, which calculates cloudy and clear sky irradiance, radiance, and transmittance, was used [*Anderson et al.*, 2000]. MODTRAN™'s historic 1 cm^{-1} band model is based on a two-parameter equivalent-width band model (proportional to temperature and pressure) that employs large prestored spectral databases. With the addition of correlated k [*Lacis and Oinas*, 1991], coupled with the automated flux output from the embedded discrete ordinate (DISORT [*Stamnes et al.*, 1988]) radiative transfer algorithm, the required inputs for this comparison are readily available. The band model parameters are derived directly from the spectral line data in HITRAN 2000 [*Rothman et al.*, 2003], including all corrections and extensions before 2004. See http://cfa-www.harvard.edu/HITRAN/ for details. The code includes the CKD [*Clough et al.*, 1980] (http://rtweb.aer.com/) continua for water vapor, O_2, and N_2, version CKD_2.4. Appropriate spectroscopic descriptions are available for each of 13 molecular species, plus cross sections for the heavy molecules (e.g., chlorofluorocarbons) in the HITRAN database. The band model approach is designed for temperature ranges between 180 and 320°K under conditions of local thermodynamic equilibrium only.

[17] MODTRAN™ provides a selection of default options for inputs, but also allows the users to supply their own. Many of the user-supplied options were used in these calculations, including some newly written options (to be included in the next release of MODTRAN™4, version 9). The MODTRAN™ calculations for this study included those in Table 2 plus (1) AOT (500 nm) converted to AOT (550 nm); (2) solar extraterrestrial irradiance, where *Gueymard* [2004] is used and differences between the MODTRAN™ default versus Gueymard are <0.2%; and (3) solar geometry, where elevation angle, as in Table 2, is converted to solar zenith angle.

Table 2. Key Model Inputs, Except for Surface Albedos, Where CST is Central Standard Time, ϖ_o is the Single Scattering Albedo, and g is the Asymmetry Parameter[a]

Case	Date	CST	Sun Elevation, deg	AOT 500 nm	α	ϖ_o	g	H_2O, cm	O_3, DU
1	5 May 2003	645	13.3	0.054	0.32	0.89	0.58	1.27	336
2		800	28.2	0.058	0.34	0.93	0.69	1.34	336
3		910	42.1	0.057	0.39	0.93	0.56	1.40	336
4		1200	68.8	0.078 (0.063)[b]	0.44	0.92	0.54	1.46	336
5		1600	38.9	0.075	0.36	0.95	0.55	1.77	336
6		1800	15.0	0.083	0.42	0.93	0.59	1.92	336
7	6 May 2003	1730	21.1	0.140	1.33	0.93	0.57	1.72	350
8		1815	12.2	0.137	1.35	0.92	0.55	1.71	350
9	7 May 2003	730	22.5	0.138	1.37	0.93	0.63	1.97	337
10		930	46.4	0.101	1.28	0.85	0.54	1.98	337
11	9 May 2003	930	46.7	0.261 (0.265)[b]	0.66	0.95	0.64	0.98	318
12		1130	67.1	0.302 (0.304)[b]	0.69	0.94	0.61	1.13	318
13		1230	70.8	0.270 (0.266)[b]	0.68	0.94	0.61	1.43	318
14	10 May 2003	700	17.0	0.487 (0.526)[b]	0.97	0.95	0.66	1.57	301
15	11 May 2003	700	17.2	0.077	1.13	0.97	0.51	1.04	312
16		920	45.1	0.084	1.15	0.97	0.57	1.09	312
17		1230	71.3	0.085 (0.055)[b]	1.04	0.94	0.58	1.14	312
18		1500	51.5	0.071 (0.057)[b]	0.97	0.96	0.55	1.13	312
19	12 May 2003	730	23.3	0.083	1.22	0.88	0.57	1.53	323
20		950	51.1	0.086 (0.080)[b]	1.23	0.93	0.56	1.54	323
21	20 May 2003	1400	63.7	0.198 (0.203)[b]	1.43	0.93	0.64	2.26	bldr-294
22	22 May 2003	800	30.4	0.194	1.42	0.94	0.66	2.43	bldr-309
23	27 May 2003	1300	73.1	0.293 (0.284)[b]	1.39	0.94	0.60	1.35	334
24		1600	41.7	0.297	1.37	0.95	0.61	1.43	334
25	28 May 2003	730	24.9	0.229	1.62	0.93	0.61	2.99	320
26		1800	17.9	0.195	1.59	0.95	0.62	2.71	320
27	29 May 2003	830	36.9	0.141	1.30	0.94	0.61	2.80	291
28		1230	75.0	0.128 (0.123)[b]	1.21	0.95	0.60	2.83	291
29	30 May 2003	1130	70.6	0.169 (0.166)[b]	1.22	0.92	0.58	3.48	293
30		1445	56.8	0.158 (0.157)[b]	1.39	0.94	0.61	3.16	293

[a]Water vapor and ozone are column values.
[b]AERONET values are in parentheses.

[18] SMARTS is the Simple Model of the Atmospheric Radiative Transfer of Sunshine. It is a clear-sky code used to calculate the shortwave (280–4000 nm) direct beam and diffuse irradiance on any surface [*Gueymard*, 1995, 2001]. It is used extensively in solar energy research and various other applications. The code is very fast, easy to run and free. The latest version (2.9.5) is used here. At each wavelength, the individual atmospheric transmittances due to absorption by a maximum of 17 gas species (besides water vapor) are calculated from Lambert-Beer's law. An optical mass specific to each species is used for it, along with temperature-dependent absorption coefficients obtained by downgrading high-resolution spectroscopic cross-section data. For water vapor, parameterizations of the MODTRAN™ band model are used. For aerosol extinction under ideal conditions, a choice of nine aerosol models is offered, thus defining all optical properties spectrally. For realistic conditions, which are the case here, Ångström's law is used to obtain AOT at any wavelength on the basis of a fit of sunphotometer data, but separately for the wave bands below and above 500 nm. To better simulate the radiometers' response, the optional circumsolar correction was turned on and a 5.7° angle was considered for both the pyrheliometer's field of view and the sky area blocked by the diffuse pyranometer's shading disk.

[19] The shortwave rapid radiative transfer model (RRTM_SW) calculates shortwave fluxes and heating rates in 14 contiguous bands [*Mlawer and Clough*, 1998; *Clough et al.*, 2004] using the correlated k method of radiative transfer and the discrete ordinates radiative transfer program DISORT [*Stamnes et al.*, 1988]. The k distributions were obtained from absorption coefficients obtained from the well-validated, line-by-line radiative transfer model LBLRTM, thus providing a traceable link from RRTM_SW to observations done at the highest spectral resolution. RRTM_SW is suitable for use as a reference to improve the performance of GCM shortwave codes. Modeled sources of extinction include water vapor, carbon dioxide, ozone, methane, oxygen, Rayleigh scattering, and aerosols. For this comparison, the aerosol optical depths are derived from the Ångstrom relationship, with spectrally constant single-scattering albedos and asymmetry parameters. The solar source function used is based on theoretical radiative transfer calculations for the solar atmosphere [*Kurucz*, 1992].

[20] Santa Barbara DISORT Atmospheric Radiative Transfer (SBDART, version 2.4) is a widely used code for calculations of radiative transfer in both cloudy and clear atmospheres [*Ricchiazzi et al.*, 1998] (http://www.crseo.ucsb.edu/esrg/pauls_dir). It is based on the DISORT multiple scattering radiative transfer module, and includes models for the important scattering and absorption processes that affect solar and infrared transmission. The code is quite flexible and provides options to run with three models of extraterrestrial source spectra, six standard atmospheric models [*McClatchey et al.*, 1972], and a variety of optical models for clouds and aerosols. To satisfy differing requirements of speed and accuracy, SBDART can be run in either the standard low-resolution mode that uses gas absorption band models from LOWTRAN, or in a more accurate

Table 3. Direct Beam Measurements and Six Model Results

Case	Direct,[a] W/m^2 (Measured)	SBDART, Direct	RAPRAD, Direct	SMARTS, Direct	SBMOD, Direct	MODTRAN, Direct	RRTM, Direct
1	604	598	607	602	602	602	597
2	**827**	811	819	813	811	812	809
3	**913**	900	909	901	899	902	898
4	**968**	950	960	954	949	952	949
5	859	851	857	853	852	842	850
6	571	568	574	568	572	569	567
7	643	650	658	650	643	647	650
8	474	478	481	479	470	475	480
9	669	666	677	666	660	664	668
10	**882**	876	886	875	872	876	876
11	757	752	763	760	754	755	755
12	798	796	806	801	796	799	798
13	816	815	826	820	815	818	817
14	263	271	277	278	264	279	275
15	681	680	690	681	674	679	682
16	910	907	916	910	902	908	909
17	971	964	972	969	960	967	967
18	936	934	943	939	931	937	937
19	750	742	752	741	738	741	744
20	909	912	921	912	908	913	914
21	854	853	862	856	847	853	855
22	694	690	698	691	684	688	692
23	844	833	840	844	827	833	835
24	732	720	727	732	713	718	721
25	**601**	600	609	600	592	597	602
26	534	531	537	536	523	526	532
27	**774**	772	779	770	768	770	773
28	**903**	898	904	900	894	897	898
29	865	857	872	858	852	856	856
30	844	843	849	844	838	841	843
Average	761.5	757.3	765.7	760.1	753.6	757.2	758.3
Measured – modeled		(0.4% lo)	0.7% hi	0.0% hi	(1.0% lo)	(0.4% lo)	(0.3% lo)

[a]Note that measurement uncertainty is about 3–4 W/m^2 for bold numbers and 8–12 W/m^2 for nonbold numbers.

correlated k mode. When running in the high-accuracy mode, SBDART uses correlated k optical depths generated from line-by-line transmission calculations. This capability was originally developed in a program named SBMOD [*Yang et al.*, 2000], which is the name used to identify the high-resolution SBDART runs in this study.

[21] For SBMOD the aerosol optical depth was interpolated between measured aerosol optical depth wavelengths. For wavelengths beyond the measured short and long wavelength endpoints an extrapolation in optical depth using an Ångstrom coefficient (α) of 1 was assumed.

4. Comparison Results

[22] Thirty clear-sky cases were selected from 13 days during the AIOP. Table 2 contains most of the input parameters used to model the direct and diffuse horizontal irradiances detected at the surface. Table 2 indicates the range of conditions that were modeled. Times ranged from early morning to late afternoon, including times near solar noon, consequently, solar elevations were as low as 12° and as high as 75°. Aerosol optical thicknesses ranged from 0.055 to 0.493 at 500 nm with some significant changes in the wavelength dependence of the aerosol extinction. A common way to express the aerosol optical depth wavelength behavior is as the slope of a linear least squares fit to a plot of the natural log of the aerosol optical depth versus the natural log of the wavelength in μm. That slope is commonly designated α, which is listed in Table 2 for all 30 cases. For comparison a typical value of α for the ARM site is 1.3 [*Michalsky et al.*, 2001]. Integrated water vapor column amounts varied between 1.0 and 3.5 cm. Ozone had a modest variation during the selected days with extreme values of 291 and 350 Dobson units. Of particular note is the fact that single scattering albedos (column labeled ϖ_o) were unexceptional with all midvisible values between 0.88 and 0.97, and most were in the middle of this range. The aerosol asymmetry parameters (column labeled g) ranged between 0.51 and 0.69.

[23] Table 3 contains the measured direct beam irradiance (the seven cavity values are in bold type in Tables 3 and 5) and the calculated results from the six models for all 30 cases. The next to last line of Table 3 is the average direct irradiance for all 30 cases. The bottom line lists the average percent difference for all thirty cases, which is different than the mean bias difference, but is used here to give equal weight to all of the cases. The six, modeled direct irradiances are from 1.0% low to 0.7% high; this range is within the estimated uncertainty in the direct irradiance measurements alone without even considering the model uncertainties. Table 4 contains the diffuse irradiance measurements and the model results for all 30 cases. Again, the mean measured and modeled irradiances are listed on the next to last line and the average percent difference from measurements for all 30 cases is on the bottom of Table 4. The range in measurement/model diffuse irradiance percent difference is between −0.6% and +1.9%. This is much smaller than the diffuse measurement uncertainty and a remarkable

Table 4. Diffuse Irradiance Measurements and Six Model Results[a]

Case	Diffuse, W/m^2 (Measured)	SBDART, Diffuse	RAPRAD, Diffuse	SMARTS, Diffuse	SBMOD, Diffuse	MODTRAN, Diffuse	RRTM, Diffuse
1	51	50	50	53	48	48	49
2	70	77	74	77	73	71	76
3	78	83	81	83	80	81	83
4	95	104	102	100	101	102	103
5	90	92	90	91	89	89	91
6	64	62	62	65	59	59	61
7	83	80	80	81	79	79	78
8	58	56	58	58	55	54	54
9	82	83	83	84	82	81	81
10	96	91	90	92	90	91	90
11	184	189	180	186	185	182	187
12	220	221	215	216	217	215	219
13	205	210	204	205	205	204	208
14	128	126	128	132	124	121	124
15	60	60	60	62	59	60	59
16	87	94	92	93	93	93	92
17	91	103	102	101	103	101	102
18	84	91	89	89	90	89	90
19	67	67	68	70	67	67	66
20	95	94	92	94	93	93	93
21	148	147	146	148	147	143	145
22	114	113	112	114	113	111	112
23	185	190	189	183	191	189	189
24	160	164	163	160	165	162	163
25	106	102	103	104	102	101	100
26	81	81	81	82	81	79	79
27	105	105	102	106	104	102	103
28	117	122	120	118	121	119	120
29	134	136	132	133	135	134	134
30	121	126	124	124	125	123	124
Average	108.6	110.6	109.1	110.1	109.2	108.1	109.2
Measured – modeled		1.8% hi	0.7% hi	1.9% hi	0.3% hi	(0.6% lo)	0.3% hi

[a]Note that measurement uncertainty is about 4 W/m^2 for numbers in first column.

improvement over earlier results, where modeled diffuse was typically 10–20% higher than measurements [*Halthore and Schwartz*, 2000; *Halthore et al.*, 2004].

[24] *Gueymard* [2003] contains a sensitivity study for direct beam only. He found that the primary contributions to uncertainty arise from aerosol optical depth and water vapor column. Table 5 contains SBDART model results and AIOP measurements with one simple change in the model inputs. The model was run with an aerosol optical depth of 0.01 subtracted from each wavelength. Using this lower aerosol optical depth, the comparison of measurements and the SBMOD model results is significantly worse with higher direct beam and lower diffuse irradiance. An uncertainty of 0.01 in aerosol optical depth is a typical one standard deviation uncertainty for well-made aerosol optical depth measurements. Of course, all inputs and radiation measurements contain uncertainty and a paper by A. McComiskey et al. (Direct aerosol forcing: Calculation from observables and sensitivities to inputs, manuscript in preparation, 2006, hereinafter referred to as McComiskey et al., manuscript in preparation, 2006) is in preparation to illustrate how uncertainties in model inputs and measurements propagate and affect both direct normal and diffuse horizontal irradiance comparisons.

5. Discussion and Conclusions

[25] The model and measurement results of Tables 3 and 4 are displayed graphically in Figure 2 (top and bottom) for direct irradiance and Figure 3 (top and bottom) for diffuse irradiance. Figures 2 (top) and 3 (top) are scatterplots of six modeled direct and diffuse irradiances, respectively, for the 30 cases versus the measured direct and diffuse irradiances. The one-to-one line is drawn in each plot to demonstrate that the correlation is high for both direct and diffuse, that the range of direct models intersect the one-to-one line in most of the thirty cases, and that the range of diffuse models intersect the one-to-one line in slightly fewer, but still the majority of cases. Figures 2 (bottom) and 3 (bottom) are plots of the differences in terms of (model – measurement) for the 30 cases in the order that they appear in Tables 3 and 4 for direct and diffuse irradiance, respectively. This latter display allows one to see amplified differences that are not obvious on the scatterplots because of the scale needed to cover the entire range of direct and diffuse irradiances for all 30 cases on those scatterplots.

[26] The results are generally encouraging in that the measurements, for the most part, fall within the range of all six models' results for both the direct and diffuse irradiance. The exceptions are clearly seen in Figures 2 (bottom) and 3 (bottom). The relatively low aerosol optical depth days (<0.10) of 5, 11, and 12 May show mixed results relative to the problem of model-overestimated diffuse for these clearest of days discussed by *Halthore and Schwartz* [2000] and *Halthore et al.* [2004]. While 5 May had the lowest aerosol optical depth, only three points of the six (cases 2–4) during the day had somewhat high diffuse values. Moreover, the direct models are low for those same points suggesting the possibility that the aerosol optical depth input values may have been high, which, if true,

Table 5. Measurement and SBDART Model Comparison With 0.01 Subtracted From the Optical Depth at Each Wavelength

Case	Direct,[a] W/m^2 (Measured)	SBDART (−0.01), Direct	Diffuse, W/m^2 (Measured)	SBDART (−0.01), Diffuse
1	604	624	51	47
2	**827**	827	70	71
3	**913**	913	78	77
4	**968**	960	95	97
5	859	864	90	86
6	571	589	64	59
7	643	666	83	76
8	474	497	58	54
9	669	682	82	79
10	**882**	887	96	86
11	757	762	184	184
12	798	804	220	216
13	816	823	205	204
14	263	279	128	125
15	681	700	60	57
16	910	918	87	87
17	971	974	91	96
18	936	946	84	84
19	750	759	67	63
20	909	922	95	88
21	854	861	148	141
22	694	702	114	109
23	844	840	185	185
24	732	729	160	160
25	**601**	612	106	99
26	534	545	81	78
27	**774**	784	105	100
28	**903**	906	117	115
29	865	865	134	130
30	844	852	121	120
Average	761.5	769.7	108.6	105.8
Measured − modeled		1.4% hi		(3.1% lo)

[a]Note that measurement uncertainty is about 3–4 W/m^2 for bold numbers and 8–12 W/m^2 for nonbold numbers.

would raise the direct and lower the diffuse. Note that the deviations on 27 May, cases 23 and 24, although not low aerosol optical depth cases, could be improved with a similar explanation. Comparing Tables 3 and 4 with Table 5 demonstrates that an optical depth of 0.01 or less could explain most of the discrepancies, and 0.01 is clearly within the uncertainty for this measurement. Nothing in Figures 2 (bottom) and 3 (bottom) suggest that 12 May results, for this low-aerosol day, are exceptional (cases 19–20). 11 May therefore appears to be the exception with three high diffuse values and no corresponding low direct values (cases 16–18). From Table 2 it appears that we could improve the diffuse comparison by using the AERONET values for aerosol optical depth, however, the modeled direct would be much too high if we were to use AERONET aerosol data.

[27] The overall modeled and measured differences for the direct beam and diffuse horizontal irradiances in terms of root-mean-square (RMS) differences and biases are summarized in Figure 4. The hatched boxes are RMS differences for direct normal and diffuse irradiances. The solid boxes represent the biases in terms of (modeled – measured) irradiances. RMS differences for direct normal irradiance range between 0.9 and 1.2%; biases range between −0.7 and 0.7%. RMS differences for diffuse irradiances range between 3.2 and 4.1%; biases range between −0.5 and 1.8%. Results for both direct and diffuse fall within the combined uncertainties of the models and measurements.

[28] The SMARTS model differs in one respect from the others in that it attempts to mimic the way measurements are actually made. Direct beam measurements include some of the solar aureole because pyrheliometers have an aperture that is either 5° or 5.7°, depending on the particular instrument, compared to the 0.5° disk subtended by the sun; diffuse measurements exclude approximately the same sized aureole. For the conditions of 10 May (large AOD and large zenith angle), this circumsolar correction was a maximum and added about 10 W/m^2 (or 3.6%) to the calculated direct normal irradiance and removed about 3 W/m^2 (or 2.2%) from the calculated diffuse horizontal irradiance.

[29] The sensitivity of the comparisons to model input and irradiance measurement uncertainties will be discussed in greater detail in a forthcoming paper (McComiskey et al., manuscript in preparation, 2006), but the change in model and measurement agreement by invoking a rather small change in optical depth as presented in the previous section illustrates the high sensitivity of these comparisons to the aerosol optical depth input. In analyzing the early comparisons among the models for this paper, it was discovered that a large difference was caused by the manner in which the models handled the aerosol optical depth wavelength dependence. Most of the models simply used an optical depth that followed the Ångstrom expression

$$\tau = \beta\lambda^{-\alpha}$$

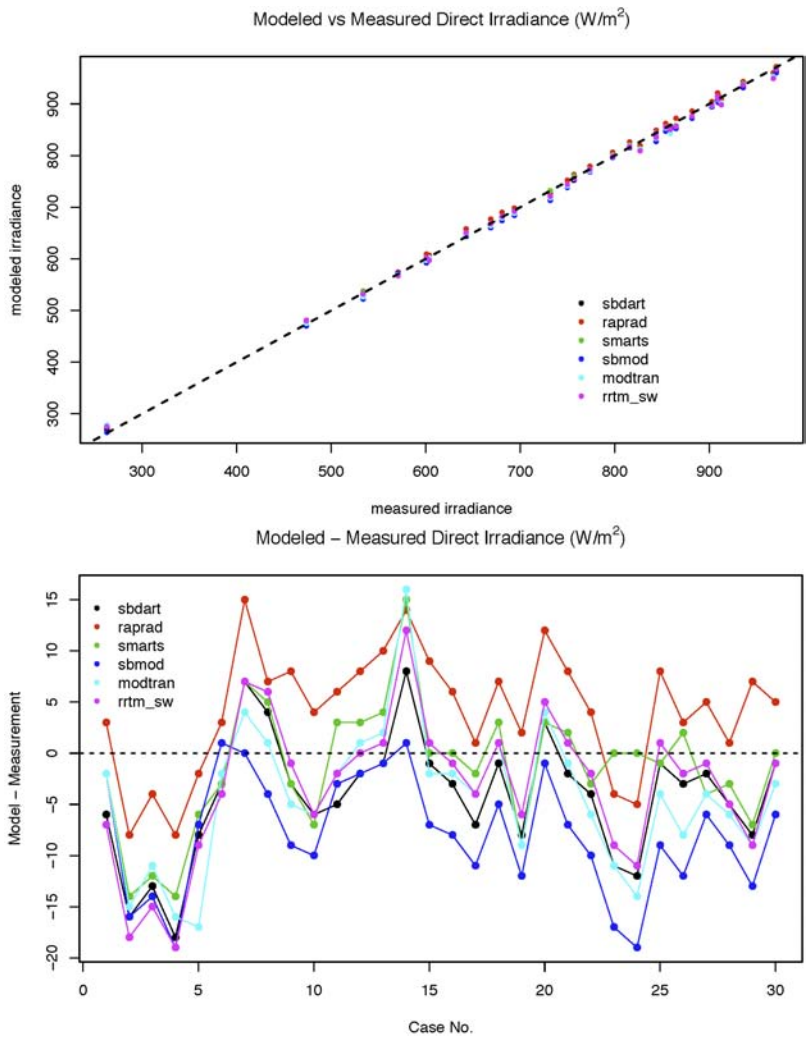

Figure 2. (top) Scatterplot of six modeled irradiances versus measured direct irradiance. (bottom). Difference plot (model – measurement) of direct irradiance as a function of case number in Table 2.

where τ is the aerosol optical depth at wavelength λ. β and α are constants based on a linear least squares fit of $\ln(\tau)$ versus $\ln(\lambda)$. The values of optical depth at 500 nm and α in Table 2 were used to calculate aerosol optical depth at all other wavelengths. SBMOD interpolates aerosol optical depth between the five NIMFR wavelengths and assumes that the aerosol optical depth at 415 nm applies to all shorter wavelengths and the aerosol optical depth at 870 nm applies at all longer wavelengths. Changing this algorithm to assume a λ^{-1} aerosol optical depth dependence outside the measured aerosol wavelength range using the 415 and 870 end points as anchors produced about a 10 W/m^2 increase in modeled direct irradiance and about a 4 W/m^2 decrease in modeled diffuse irradiance yielding significant improvements in the agreement with measured values.

[30] In general, the extinction of real aerosols cannot be described using fixed aerosol models from the literature. Therefore the SMARTS model uses its built-in simplified treatment based on the AOD at 500 nm and a two-tier Ångstrom law, with distinct average values of the wavelength exponent (α) for the 280–500 and 500–4000 nm wave bands. This was specifically done here by linearly fitting the measured aerosol optical depth values from the five available NIMFR channels (415–870 nm) to the log-transformed Ångstrom's equation, separately for these two wave bands. The broadband-averaged alpha value indicated in Table 2 was, therefore, not used for SMARTS runs. Note, however, that the two band-average values of α obtained were generally found close to each other for all days except 5 May, when the 280–500 nm α was negative and considerably smaller in magnitude than the positive 500–4000 nm α; this behavior in aerosol optical depth wavelength dependence indicates an atypical mix of aerosols on that day.

[31] Referring to Table 1, the surface albedos were treated differently in the six models. Files of surface albedo were supplied for the 300–3000 nm range. Most models simply used the values at 300 nm and 3000 nm for wavelengths shorter and longer than these wavelengths, respectively. Some models set the values outside the given range to zero. For clear skies these assumptions will make no difference in direct beam results and little difference in diffuse irradiance given the small contribution of midinfrared radiation in clear skies and the small contribution of ultraviolet radiation below 300 nm in all skies. Surface albedos at the six fixed

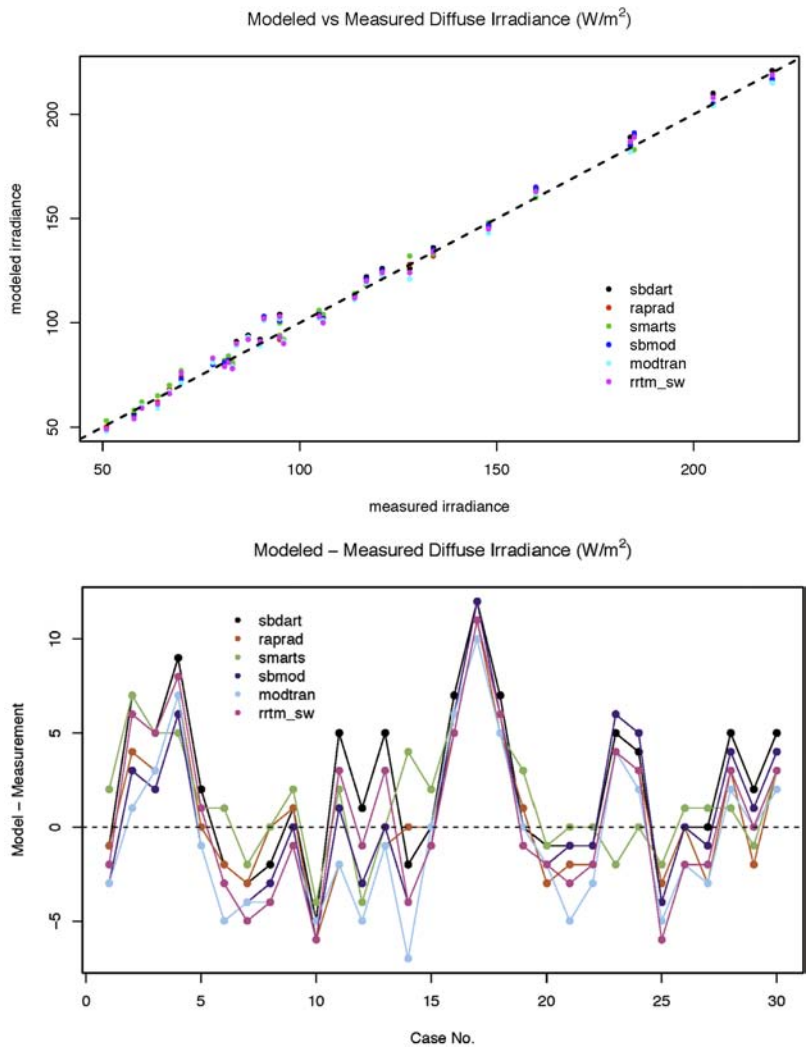

Figure 3. (top) Scatterplot of six modeled irradiances versus measured diffuse irradiance. (bottom). Difference plot (model – measurement) of diffuse irradiance as a function of case number in Table 2.

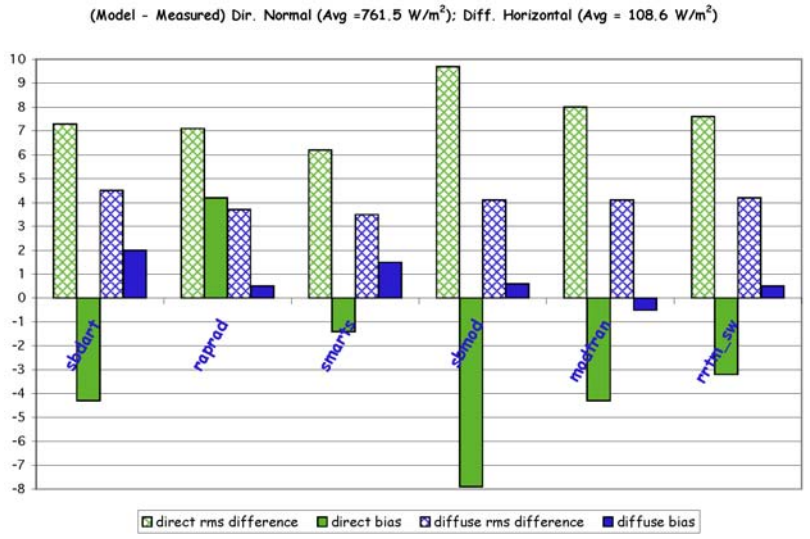

Figure 4. Thirty cases of (modeled – measured) results in W/m^2 for direct beam and diffuse horizontal irradiances.

wavelengths, which were used to parameterize the surface albedo for the full range of wavelengths in the input files, were also made available for the model runs. One model was run using those measured values directly, linearly interpolating between the measurements and using the endpoint albedos for wavelengths outside the range of the measurements. This resulted in less than a 0.1% change in diffuse irradiance. More significantly, if the surface albedo is derived from the measured broadband surface albedo and that constant value is used for all wavelengths, the calculated diffuse irradiance is larger, on average, by 7%.

[32] Since ground-based values of single scattering albedo and asymmetry parameter were used, it can be argued that the column values of these parameters may not be well represented in these calculations. *Andrews et al.* [2004] found that the ground-based measurements at the AOS are, on average, fairly representative of the column. If anything, the column-averaged single scattering albedo tends to be slightly lower than the surface value for an average profile. A lower single scattering albedo would slightly reduce the diffuse model results. The asymmetry parameter tends to be greater in the layers just above the surface and then smaller at even higher altitudes, thus it is less clear whether the column-averaged asymmetry parameter would produce any difference in modeled diffuse irradiance at the surface (E. Andrews, private communication, 2006). During the AIOP, elevated layers of aerosol above the site were detected. In the last days of the month these aerosol layers originated from Siberian forest fires. *Ferrare et al.* [2006] report single scattering albedos of 0.96–0.98 for these elevated aerosol layers on 25 and 27 May. These values are slightly, but not significantly greater than the surface-based AOS single scattering albedos; therefore they should not significantly affect the calculated diffuse irradiance.

[33] Only one model used a significantly different wavelength range to define the shortwave. SBMOD's longwave cutoff was 2950 nm, while the other models included radiation out to 3800 nm or beyond. On the basis of a MODTRAN™ sensitivity run, a cutoff at 3000 nm should result in direct being underestimated, relative to a longwave cutoff of 4000 nm, by 5–6 W/m^2 on average and produce less than a 0.5 W/m^2 underestimate in diffuse. Therefore, if the shortwave cutoff were extended to 4000 nm we would expect the SBMOD direct model and measurement difference to improve significantly, with the diffuse overestimate changing modestly. Only one model RRTM_SW did not use the *Gueymard* [2004] extraterrestrial spectrum; it used the *Kurucz* [1992] theoretical spectrum that integrates to 1368 W/m^2, which is 2 W/m^2 larger than *Gueymard* [2004]. Using the latter spectrum one would expect the RRTM_SW direct bias to increase by about 1 W/m^2.

[34] In summary, solar radiation models and measurements seem to have merged as a result of better specification of input parameters and better measurements of irradiances than in prior studies. However, improving the uncertainties of the inputs and irradiance measurements is an unfinished task. Further effort is warranted in testing more cases for very low aerosol optical depth days that tend to occur in mid to late autumn at the SGP CRF. Finally, these models should be tested spectrally against a carefully calibrated shortwave spectral irradiance data set in order to ensure that cancellation of errors in different portions of the spectrum is not responsible for the excellent agreement achieved in this study.

[35] **Acknowledgments.** We thank Mary Jane Bartholomew for providing the CIMEL aerosol optical depths for comparison to the NIMFR data. Alexander Berk provided assistance with regard to setting up the MODTRAN™ calculations. John Augustine carefully edited the final version. NOAA's Climate Program supported this work as did the Office of Science (BER), U.S. Department of Energy, through Interagency Agreement DE-AI02-04ER63703. The AIOP was made possible through the financial support of the U.S. Department of Energy's Atmospheric Radiation Measurement program.

References

Anderson, G. P., et al. (2000), MODTRAN4: Radiative transfer modeling for remote sensing in algorithms for multispectral, hyperspectral, and ultraspectral imagery VI, *Proc. SPIE Int. Soc. Opt. Eng.*, *4049*, 176–183.

Andrews, E., P. J. Sheridan, J. A. Ogren, and R. Ferrare (2004), In situ aerosol profiles over the Southern Great Plains cloud and radiation test bed site: 1. Aerosol optical properties, *J. Geophys. Res.*, *109*, D06208, doi:10.1029/2003JD004025.

Andrews, E., et al. (2006), Comparison of methods for deriving aerosol asymmetry parameter, *J. Geophys. Res.*, *111*, D05S04, doi:10.1029/2004JD005734.

Barnard, J. C., and D. M. Powell (2002), A comparison between modeled and measured clear-sky radiative shortwave fluxes in Arctic environments, with special emphasis on diffuse radiation, *J. Geophys. Res.*, *107*(D19), 4383, doi:10.1029/2001JD001442.

Bush, B. C., F. P. J. Valero, A. S. Simpson, and L. Bignone (2000), Characterization of thermal effects in pyranometers: A data correction algorithm for improved measurement of surface insolation, *J. Atmos. Oceanic Technol.*, *17*, 165–175.

Clough, S. A., F. X. Kneizys, R. Davis, R. Gamache, and R. Tipping (1980), Theoretical line shape for H_2O vapor: Application to the continuum, in *Atmospheric Water Vapor*, edited by A. Deepak, T. D. Wilkerson, and L. H. Ruhnke, pp. 25–47, Elsevier, New York.

Clough, S. A., M. W. Shephard, E. J. Mlawer, J. S. Delamere, M. J. Iacono, K. Cady-Pereira, S. Boukabara, and P. D. Brown (2004), Atmospheric radiative transfer modeling: A summary of the AER codes, *J. Quant. Spectrosc. Radiat. Transfer*, *91*, 233–244.

d'Almeida, G. A., P. Koepke, and E. P. Shettle (1991), *Atmospheric Aerosols: Global Climatology and Radiative Characteristics*, 561 pp., A. Deepak, Hampton, Va.

Dutton, E. G., J. J. Michalsky, T. Stoffel, B. W. Forgan, J. Hickey, D. W. Nelson, T. L. Alberta, and I. Reda (2001), Measurement of broadband diffuse solar irradiance using current commercial instrumentation with a correction for thermal offset errors, *J. Atmos. Oceanic Technol.*, *18*, 297–314.

Ferrare, R., et al. (2006), Evaluation of daytime measurements of aerosols and water vapor made by an operational Raman lidar over the Southern Great Plains, *J. Geophys. Res.*, *111*, D05S08, doi:10.1029/2005JD005836.

Goody, R. M., and Y. L. Yung (1989), *Atmospheric Radiation*, 2nd ed., Oxford Univ. Press, New York.

Gueymard, C. (1995), SMARTS2, Simple Model of the Atmospheric Radiative Transfer of Sunshine: Algorithms and performance assessment, *Rep. FSEC-PF-270-95*, Fla. Sol. Energy Cent., Cocoa Beach, Fla.

Gueymard, C. (2001), Parameterized transmittance model for direct beam and circumsolar spectral irradiance, *Sol. Energy*, *71*, 325–346.

Gueymard, C. A. (2003), Direct solar transmittance and irradiance predictions with broadband models. Part II: validation with high-quality measurements, *Sol. Energy*, *74*, 381–395, (Corrigendum, *Sol. Energy, 76,* 515, 2004.).

Gueymard, C. A. (2004), The sun's total and spectral irradiance for solar energy applications and solar radiation models, *Sol. Energy*, *76*, 423–453.

Gulbrandsen, A. (1978), On the use of pyranometers in the study of spectral solar radiation and atmospheric aerosols, *J. Appl. Meteorol.*, *17*, 899–904.

Haeffelin, M., S. Kato, A. M. Smith, C. K. Rutledge, T. P. Charlock, and J. R. Mahan (2001), Determination of the thermal offset of the Eppley precision spectral pyranometer, *Appl. Opt.*, *40*, 472–484.

Halthore, R. N., and S. E. Schwartz (2000), Comparison of model-estimated and measured diffuse downward irradiance at surface in cloud-free skies, *J. Geophys. Res.*, *105*, 20,165–20,177.

Halthore, R. N., S. E. Schwartz, J. J. Michalsky, G. P. Anderson, R. A. Ferrare, B. N. Holben, and H. M. Ten Brink (1997), Comparison of

model estimated and measured direct-normal solar irradiance, *J. Geophys. Res.*, *102*, 29,991–30,002.

Halthore, R. N., S. Nemesure, S. E. Schwartz, D. G. Emre, A. Berk, E. G. Dutton, and M. H. Bergin (1998), Models overestimate diffuse clear-sky irradiance: A case for excess atmospheric absorption, *Geophys. Res. Lett.*, *25*, 3591–3594.

Halthore, R. N., M. A. Miller, J. A. Ogren, P. J. Sheridan, D. W. Slater, and T. Stoffel (2004), Further developments in closure experiments for diffuse irradiance under cloud-free skies at a continental site, *Geophys. Res. Lett.*, *31*, L07111, doi:10.1029/2003GL019102.

Harrison, L., J. Michalsky, and J. Berndt (1994), Automated multifilter rotating shadow-band radiometer: An instrument for optical depth and radiation measurements, *Appl. Opt.*, *33*, 5118–5125.

Henzing, J. S., W. H. Knap, P. Stammes, A. Apituley, J. B. Bergwerff, D. P. J. Swart, G. P. A. Kos, and H. M. ten Brink (2004), Effect of aerosols on the downward shortwave irradiances at the surface: Measurements versus calculations with MODTRAN4.1, *J. Geophys. Res.*, *109*, D14204, doi:10.1029/2003JD004142.

Holben, B. N., et al. (1998), AERONET—A federated instrument network and data archive for aerosol characterization, *Remote Sens. Environ.*, *66*, 1–16.

Kato, S., T. P. Ackerman, E. E. Clothiaux, J. H. Mather, G. G. Mace, M. L. Wesely, F. Murcray, and J. Michalsky (1997), Uncertainties in modeled and measured clear-sky surface shortwave irradiances, *J. Geophys. Res.*, *102*, 25,881–25,898.

Kato, S., T. P. Ackerman, J. H. Mather, and E. E. Clothiaux (1999), The k-distribution method and correlated-k approximation for a shortwave radiative transfer model, *J. Quant. Spectrosc. Radiat. Transfer*, *62*, 109–121.

Kurucz, T. L. (1992), Synthetic infrared spectra, in *Infrared Solar Physics, IAU Symposium 154*, edited by D. M. Rabin and J. T. Jeffries, pp. 523–531, Springer, New York.

Lacis, A. A., and V. Oinas (1991), A description of the correlated-k distribution method for modeling non-gray gaseous absorption, thermal emission, and multiple scattering in vertically inhomogeneous atmospheres, *J. Geophys. Res.*, *96*, 9027–9063.

Liljegren, J. C. (1994), Two-channel microwave radiometer for observations of total column precipitable water vapor and cloud liquid water path, paper presented at Fifth Symposium on Global Climate Change Studies, Am. Meteorol. Soc., Nashville, Tenn., 25–28 Jan.

Liljegren, J. C., S. A. Boukabara, K. Cady-Pereira, and S. A. Clough (2005), The effect of the half-width of the 22-ghz water vapor line on the retrievals of temperature and water vapor profiles with a twelve-channel microware radiometer, *IEEE Trans. Geosci. Remote Sens.*, *43*, 1102–1108.

McClatchey, R. A., R. W. Fenn, J. E. A. Selby, F. E. Volz, and J. S. Garing (1972), *Optical Properties of the Atmosphere*, 3rd ed., Air Force Cambridge Res. Lab., L.G. Hanscom Field, Bedford, Mass.

Michalsky, J. J., J. A. Schlemmer, W. E. Berkheiser, J. L. Berndt, L. C. Harrison, N. S. Laulainen, N. R. Larson, and J. C. Barnard (2001), Multiyear measurements of aerosol optical depth in the Atmospheric Radiation Measurement and Quantitative Links programs, *J. Geophys. Res.*, *106*(D11), 12,099–12,108.

Michalsky, J. J., et al. (2003a), Results from the first ARM diffuse horizontal shortwave irradiance comparison, *J. Geophys. Res.*, *108*(D3), 4108, doi:10.1029/2002JD002825.

Michalsky, J., Q. Min, J. Barnard, R. Marchand, and P. Pilewskie (2003b), Simultaneous spectral albedo measurements near the Atmospheric Radiation Measurement Southern Great Plains (ARM SGP) central facility, *J. Geophys. Res.*, *108*(D8), 4254, doi:10.1029/2002JD002906.

Michalsky, J. J., et al. (2005), Toward the development of a diffuse horizontal shortwave irradiance working standard, *J. Geophys. Res.*, *110*, D06107, doi:10.1029/2004JD005265.

Mlawer, E. J., and S. A. Clough (1998), Shortwave clear-sky model-measurement intercomparison using RRTM, paper presented at Eighth ARM Science Team Meeting, U.S. Dep. of Energy, Tucson, Ariz., 23–27 Mar.

Ricchiazzi, P., S. Yang, C. Gautier, and D. Sowle (1998), SBDART: A research and teaching software tool for plane-parallel radiative transfer in the Earth's atmosphere, *Bull. Am. Meteorol. Soc.*, *79*, 2101–2114.

Rothman, L. S., et al. (2003), The HITRAN molecular spectroscopic database: Edition of 2000 including updates through 2001, *J. Quant. Spectrosc. Radiat. Transfer*, *82*, 5–44.

Schmid, B., J. Michalsky, R. Halthore, M. Beauharnois, L. Harrison, J. Livingston, P. Russell, B. Holben, T. Eck, and A. Smirnov (1999), Comparison of aerosol optical depth from four solar radiometers during the fall 1997 ARM Intensive Observation Period, *Geophys. Res. Lett.*, *26*, 2725–2728.

Schmid, B., et al. (2006), How well can we measure the vertical profile of tropospheric aerosol extinction?, *J. Geophys. Res.*, *111*, D05S07, doi:10.1029/2005JD005837.

Sheridan, P. J., D. J. Delene, and J. A. Ogren (2001), Four years of continuous surface aerosol measurements from the Department of Energy's Atmospheric Radiation Measurement Program Southern Great Plains Cloud and Radiation Testbed site, *J. Geophys. Res.*, *106*, 20,735–20,747.

Sheridan, P. J., A. Jefferson, and J. A. Ogren (2002), Spatial variability of submicrometer aerosol radiative properties over the Indian Ocean during INDOEX, *J. Geophys. Res.*, *107*(D19), 8011, doi:10.1029/2000JD000166.

Stamnes, K., S. C. Tsay, W. J. Wiscombe, and K. Jayaweera (1988), Numerically stable algorithm for discrete-ordinate-method raditive transfer in multiple scattering and emitting layered media, *Appl. Opt.*, *27*, 2502–2509.

Toon, O. B., C. P. Mckay, T. P. Ackerman, and K. Santhanam (1989), Rapid calculation of radiative heating rates and photodissociation rates in inhomogeneous multiple scattering atmosphere, *J. Geophys. Res.*, *94*, 16,287–16,301.

Wiscombe, W. J., and G. W. Grams (1976), The backscattered fraction in two-stream approximations, *J. Atmos. Sci.*, *33*, 2440–2451.

Yang, S. R., P. Ricchiazzi, and C. Gautier (2000), Modified correlated k-distribution methods for remote sensing applications, *J. Quant. Spectrosc. Radiat. Transfer*, *64*(6), 585–608.

G. P. Anderson, Air Force Research Laboratory/Battlespace Surveillance Innovation Center, U.S. Air Force, 325 Broadway, R/GMD2, Boulder, CO 80305, USA. (gail.anderson@noaa.gov)

J. Barnard, Pacific Northwest National Laboratory, Richland, WA 99352, USA. (james.barnard@pnl.gov)

J. Delamere, Atmospheric and Environmental Research, Inc., Lexington, MA 02421-3136, USA. (jdelamer@aer.com)

C. Gueymard, Solar Consulting Services, Inc., P.O. Box 392, Colebrook, NH 03576, USA. (chris@solarconsultingservices.com)

S. Kato, Center for Atmospheric Sciences, Hampton University, Hampton, VA 23668, USA. (s.kato@larc.nasa.gov)

P. Kiedron, Atmospheric Sciences Research Center, State University of New York, Albany, NY 12222, USA. (kiedron@asrc.cestm.albany.edu)

A. McComiskey, Cooperative Institute for Research in Environmental Sciences, University of Colorado, Boulder, CO 80309, USA. (allison.mccomiskey@noaa.gov)

J. J. Michalsky, Earth System Research Laboratory, NOAA, Boulder, CO 80305, USA. (joseph.michalsky@noaa.gov)

P. Ricchiazzi, Institute for Computational Earth System Science, University of California, Santa Barbara, CA 93106, USA. (paul@icess.ucsb.edu)